


## Article

# Theoretical and Experimental Analysis on Statistical Properties of Coupling Efficiency for Single-Mode Fiber in Free-Space Optical Communication Link Based on Non-Kolmogorov Turbulence

Lie Ma <sup>1,2</sup>, Shijie Gao <sup>1,\*</sup>, Bo Chen <sup>1</sup> and Yongkai Liu <sup>1</sup> 

<sup>1</sup> Changchun Institute of Optics, Fine Mechanics and Physics, Chinese Academy of Sciences, Changchun 130033, China; hitmalie@126.com (L.M.); chenb@ciomp.ac.cn (B.C.); liuyk@ciomp.ac.cn (Y.L.)

<sup>2</sup> University of Chinese Academy of Sciences, Beijing 100049, China

\* Correspondence: gaoshijie@ciomp.ac.cn; Tel.: +86-0431-8670-8235

**Abstract:** Non-Kolmogorov turbulence has been widely observed in free-space optical communication links and should be used to evaluate the system performance. We calculated the wavefront residual variance in the condition of the non-Kolmogorov turbulence model and deduced the mathematical expression of the probability density function (PDF) for the coupling efficiency (CE) of a single-mode fiber (SMF). The PDF was simulated, and the results showed its robustness and rationality. Moreover, an experiment was set up to verify the PDF with experimental distribution. The correlation coefficients are above 0.95 in all cases, which means the statistical model of the CE fitted the experimental distribution well.

**Keywords:** free-space optical communication; non-Kolmogorov turbulence; probability density function; coupling efficiency



**Citation:** Ma, L.; Gao, S.; Chen, B.; Liu, Y. Theoretical and Experimental Analysis on Statistical Properties of Coupling Efficiency for Single-Mode Fiber in Free-Space Optical Communication Link Based on Non-Kolmogorov Turbulence. *Appl. Sci.* **2022**, *12*, 6075. <https://doi.org/10.3390/app12126075>

Academic Editors: Amalia Miliou and Petr Münster

Received: 12 May 2022

Accepted: 14 June 2022

Published: 15 June 2022

**Publisher's Note:** MDPI stays neutral with regard to jurisdictional claims in published maps and institutional affiliations.



**Copyright:** © 2022 by the authors. Licensee MDPI, Basel, Switzerland. This article is an open access article distributed under the terms and conditions of the Creative Commons Attribution (CC BY) license (<https://creativecommons.org/licenses/by/4.0/>).

## 1. Introduction

Free-space optical communication (FSO) technology is applied widely in satellite-ground, satellite-satellite and other communication links [1,2] for its small size, low power cost, high reliability and security [3]. Considering the atmospheric channel, turbulence is one of the most important factors that influence system performance. The wavefront of the signal light at the receiving telescope will distort heavily, and the parameters, which are used to evaluate system performance, turn into random variables because of the randomness of turbulence.

The Kolmogorov turbulence model is used extensively in considering the turbulence effect of the atmosphere for its simple mathematical structure and usability for numerical calculation [4–6]. However, with the increase of theoretical discussion and experimental research [7–9], it has been found that Kolmogorov's theory could not always describe the characteristics of actual turbulence, and the non-Kolmogorov turbulence model has been widely applied to evaluate the performance of FSO terminals. Linyan Cui studied the influence of moderate-to-strong non-Kolmogorov turbulence on the imaging system based on the atmospheric turbulence modulation transfer function [10]. Yahya Baykal investigated the behavior of the coherence length in non-Kolmogorov satellite links [11]. Moreover, JR Yao generalized the oceanic spatial power spectrum to the non-Kolmogorov turbulence regime based on temperature and salinity concentration [12].

Signal light received by FSO terminals is usually coupled into an Erbium-doped optical fiber amplifier (EDFA) for next processing, especially in a coherent communication system, in order to achieve a high data rate [13], so the coupling progress becomes one of the interests [14–16]. Therefore, coupling efficiency (CE) is one of the most important parameters to evaluate the performance of communication terminals and should be well discussed in the conditions of non-Kolmogorov turbulence.

The mean value and variance of the CE are two essential parameters to evaluate system performance because some system indicators are directly associated with CE. Moreover, non-linear relationships widely exist between the CE and these indicators [17]. For example, the signal-to-noise ratio (SNR) is proportional to the square of the receiving power in the IM/DD system. The receiving power is linear to the CE, so the SNR is non-linear to the CE. Thus, the statistical model of CE should be built to analyze the mean value and fluctuation of these indicators affected by turbulence [18]. Chao and Liying discussed the CE of a Gauss beam transmitting through non-Kolmogorov turbulence and gave the expression of the CE. However, it was a complex double integral and not convenient for further discussion of the system performance for FSO terminals [19]. They also discussed a fiber CE based on non-Kolmogorov theory in a satellite-ground link, and showed the trends, but did not study its statistical characteristics [20]. Beibei Hu and Ying Xu gave us an expression of the CE for a partially coherent laser beam propagating through non-Kolmogorov turbulence. This also ended up with an integral with no analytic solution [21]. Moreover, Xin Zhao and Huilin Jiang discussed the CE on focal plane spot extension caused by turbulence. The results showed that CE was related to aperture, the wavelength of incident light, the radius of the receiving fiber, the atmosphere coherence length and the coupling system focus length, but they did not discuss the influence when different turbulence models were chosen [22]. Chao Wang and Lun Jiang studied the CE of a Gaussian beam passing through weak fluctuation regimes. However, the results were based on Kolmogorov turbulence [23]. Mo Chen and Chao Liu analyzed the influence of the atmospheric turbulence on the SMF coupling efficiency over various turbulences. They verified that the adaptive optics system was one of the most effective methods to improve the FSO system performance. However, they only took the average CE as the performance indicator and did not analyze its distribution [24]. Yiming Bian and Yan Li analyzed the CE in the condition of an optical system aberration and fiber positioning error. They only considered the influence of the effects caused by turbulence and did not discuss the randomness of the CE due to turbulence [25]. As shown in Table 1, all the researchers do not derive an analytical expression of the CE effected by atmospheric turbulence, and the statistical characteristics are not discussed.

**Table 1.** Study comparison.

	Ref.	[19]	[20]	[21]	[22]	[23]	[24]	[25]
Study type	Theory	✓	✓	✓	✓	✓	✓	✓
	Simulation	✓	✓	✓	✓	✓	✓	✓
	Experiment	-	-	-	-	-	✓	-
Turbulence model	Kolmogorov	-	-	-	✓	✓	✓	✓
	Non-Kolmogorov	✓	✓	✓	-	-	-	-
Result form	Analytical expression	-	-	-	-	-	-	-
	Complex integral	✓	✓	✓	✓	✓	✓	✓
	Statistical distribution of CE	-	-	-	-	-	-	-

In this study, we created a new statistical model of the CE based on non-Kolmogorov turbulence and derived the analytical expression of the PDF. The spectral power law was introduced as a variable to correct the variance of the wavefront error, so that the PDF could fit the actual distribution. The foundation is to evaluate system performance using a statistical method, whether the parameter is linear to the CE or not. We also simulated the model in different conditions. Compared with the model based on the Kolmogorov model, the results showed its rationality and robustness. In addition, an experiment was designed to collect the CE data affected by actual turbulence. We counted the distribution and compared it with the model we built. The results showed that the model based on non-Kolmogorov turbulence could describe the experimental distribution well in all cases.

We provide the modeling progress in Section 2, in which the calculation of variance of the wavefront error and the detailed derivation of the PDF are listed. The simulation

analysis is presented in Section 3, and the experimental verification with its analysis are shown in Section 4. Section 5 is the conclusion of this study.

### 2. Theoretical Analysis

The Kolmogorov atmosphere model is widely used to describe turbulence in free-space laser communication links, but it is not accurate because the boundary conditions are not always satisfied [26,27]. The statistical model of the wavefront based on non-Kolmogorov turbulence is essential to evaluate the PDF of the CE for SMF.

Figure 1 shows the optical structure of a free-space optical communication terminal and how special signal light couples into SMF. Signal and beacon light propagate through the atmosphere and are affected by atmospheric turbulence. Both of them are received by the optical antenna, which consists of a telescope. It is designed to minimize the radius of the signal light at the optical pupil and beneficial to minimize the optical structure. The telescope is set on the coarse tracking element to follow the beacon light. Reflected by the fast steering mirror (FSM), which is the fine tracking element, the beacon and signal light are separated by the beam splitter 1 (BS1). The beacon light is received by the coarse tracking camera, which provides the feedback signal for the coarse tracking element. The signal light transmits through the beam splitter 2 (BS2), which splits the receiving and launching signal, and splits them with the beam splitter 3 (BS3). Most of the energy, e.g., 95%, is coupled into the SMF by the coupling optical system for the next processing, while the rest transmits into the fine tracking camera, providing the feedback signal for the FSM. Therefore, the CE is essential to evaluate the performance of the receiving terminal.

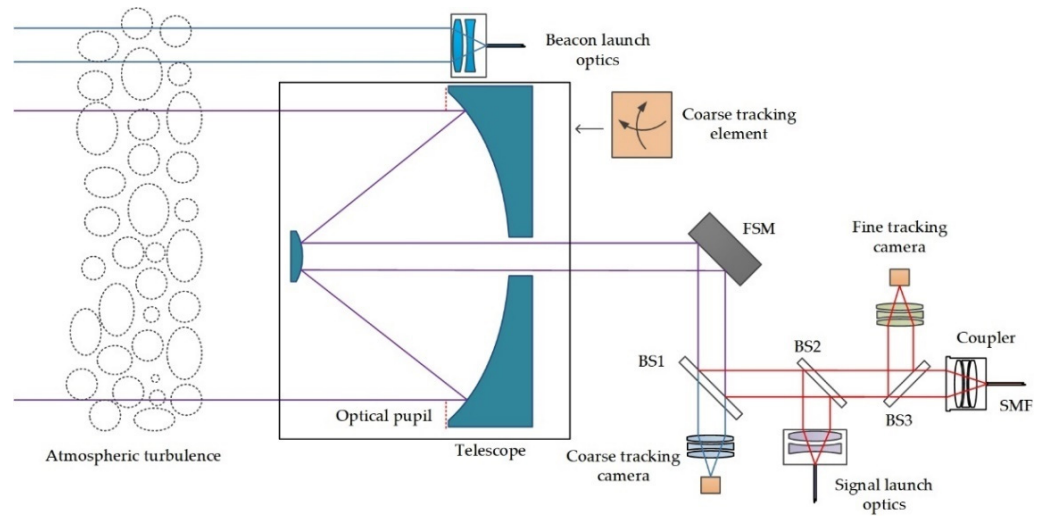


**Figure 1.** Free-space signal light couples into a single-mode fiber.

Firstly, the wavefront residual variance based on the non-Kolmogorov model is calculated. Zernike polynomials are widely used to expand the random wavefront. Considering a plane where a random wavefront is expanded, a polar coordinate system is needed. Here,  $r$  represents the polar radius and  $\theta$  is for the polar angle. Zernike polynomials are defined by Equation (1) [28]

$$\begin{aligned} Z_{even\ j} &= \sqrt{(n+1)R_n^m(r)}\sqrt{2}\cos m\theta, \quad m \neq 0 \\ Z_{odd\ j} &= \sqrt{(n+1)R_n^m(r)}\sqrt{2}\sin m\theta, \quad m \neq 0 \\ Z_j &= \sqrt{(n+1)R_n^0(r)}, \quad m = 0 \end{aligned} \tag{1}$$

where,

$$R_n^m(r) = \sum_s^{(n-m)/2} \frac{(-1)^s (n-s)!}{s! \left[\frac{n+m}{2} - s\right]! \left[\frac{n-m}{2} - s\right]!} r^{n-2s} \tag{2}$$

where  $n$  and  $m$  are integral and satisfy  $m \leq n$ ,  $n - |m| = \text{even}$  and  $j$  is a mode-ordering number which is the function of  $n$  and  $m$ . Table 2 shows the first 10 polynomials.

**Table 2.** First 10 items of Zernike polynomials.

$n \backslash m$	0	1	2	3
0	$Z_1 = 0$			
1		$Z_2 = 2r \cos \theta$	$Z_3 = 2r \sin \theta$	
2	$Z_3 = \sqrt{3}(2r^2 - 1)$		$Z_5 = \sqrt{6}r^2 \sin 2\theta$ $Z_6 = \sqrt{6}r^2 \cos 2\theta$	
3		$Z_7 = 2\sqrt{2}(3r^3 - 2r) \sin \theta$ $Z_8 = 2\sqrt{2}(3r^3 - 2r) \cos \theta$		$Z_9 = 2\sqrt{2}r^3 \sin 3\theta$ $Z_{10} = 2\sqrt{2}r^3 \cos 3\theta$

It is convenient to use Zernike polynomials expanding a random wavefront  $\phi(r, \theta)$ , given by Equations (3)–(5).

$$\phi(r, \theta) = \sum_j a_j Z_j(r, \theta) \tag{3}$$

$$a_j = \frac{1}{R^2} \int W\left(\frac{r}{R}\right) \phi(r, \theta) Z_j\left(\frac{r}{R}, \theta\right) d^2r \tag{4}$$

$$W(r) = \begin{cases} \frac{1}{\pi} & r \leq 1 \\ 0 & r > 1 \end{cases} \tag{5}$$

The more terms we use in Equation (3), the more accurately will the wavefront be described. However, we can only expand the wavefront with finite Zernike terms, so the mean square residual error  $\Delta_J$  should be well discussed, which is shown in Equation (6).

$$\Delta_J = \langle \phi^2 \rangle - \sum_{j=1}^J \langle |a_j|^2 \rangle \tag{6}$$

$\langle |a_j|^2 \rangle$  represents the Zernike coefficient variances and  $\langle \phi^2 \rangle$  is total wavefront error shown by Equation (7).

$$\langle \phi^2 \rangle = \sum_{j=1}^{\infty} \langle |a_j|^2 \rangle \tag{7}$$

Consider the distorted wavefront effected by non-Kolmogorov turbulence. The three-dimensional power spectral density of phase fluctuations is

$$\Phi_{\phi}(k) = \frac{A_{\beta} k^{-\beta}}{r_0^{\beta-2}} \tag{8}$$

$\beta$  is the power law at the range from 2 to 4. When it equals to 11/3,  $\Delta_J$  has the same value of the residual variance based on the Kolmogorov model [29].  $A_{\beta}$  is a coefficient related to  $\beta$ , which has the value that  $\Delta_1$  is normalized to 1 rad<sup>2</sup> when the diameter of receiving aperture equals to  $r_0$ , given by Equation (9) [29].

$$A_{\beta} = \frac{2^{\beta-2} \left[ \Gamma\left(\frac{\beta+2}{2}\right) \right]^2 \Gamma\left(\frac{\beta+4}{2}\right) \Gamma\left(\frac{\beta}{2}\right) \sin\left(\pi \frac{\beta-2}{2}\right)}{\pi^{\beta} \Gamma(\beta+1)} \tag{9}$$

According to the definition of  $a_j$  and the  $A_{\beta}$ , the Zernike coefficient variances  $\langle |a_j|^2 \rangle$  are given by Equation (10).

$$\langle |a_j|^2 \rangle = \left(\frac{D}{r_0}\right)^{\beta-2} \frac{(n+1)}{\pi} \frac{\Gamma\left(\frac{2n+2-\beta}{2}\right)\Gamma\left(\frac{\beta+4}{2}\right)\Gamma\left(\frac{\beta}{2}\right)\sin\left(\pi\cdot\frac{\beta-2}{2}\right)}{\Gamma\left(\frac{2n+4+\beta}{2}\right)} \tag{10}$$

Substitute Equations (7) and (10) for Equation (6), and  $\Delta_J$  is calculated.

We assume that the field of SMF could transfer backwards to the pupil plane of the receiving telescope, at which the coupling is processed and in which the condition of the CE is defined by Equations (11) and (12).  $E_A(r)$  represents the optical field of the signal light at the pupil plane, which is a plane-wave function.  $F_A(r)$  is the model field of the SMF transferring backwards to the pupil plane, and it is a Gaussian function, approximately.  $\chi$  is an intermediate variable, and  $\chi_r$  and  $\chi_i$  represent the real and imaginary parts of  $\chi$ . Considering atmospheric turbulence,  $\phi$  turns into a random variable and is related to  $r$ , so the integrals in Equations (11) and (12) have no analytic solution.

$$\eta = \frac{|\int \int E_A^*(r)F_A(r)drd\phi|^2}{|\int \int E_A(r)drd\phi|^2|\int \int F_A(r)drd\phi|^2} = \frac{2}{\pi^2 R^2 \omega_a^2} (\chi_r^2 + \chi_i^2) \tag{11}$$

$$\begin{cases} \chi_r = \int \int \exp\left(-\frac{r^2}{\omega_a^2}\right) \cos \phi drd\phi = \sqrt{\chi^2} \cos \theta \\ \chi_i = \int \int \exp\left(-\frac{r^2}{\omega_a^2}\right) \sin \phi drd\phi = \sqrt{\chi^2} \sin \theta \\ \chi^2 = \chi_r^2 + \chi_i^2 \end{cases} \tag{12}$$

If we get the PDF of  $\chi^2$ , which is  $p_{\chi^2}(\chi^2)$ , the PDF of the CE could be described as Equation (13), based on Equation (11).

$$p_H(\eta) = \frac{\pi^2 R^2 \omega_a^2}{2} p_{\chi^2} \left( \frac{\pi^2 R^2 \omega_a^2}{2} \chi^2 \right) \tag{13}$$

When the signal light reaches the pupil of the receiving telescope after transmitting through the atmospheric turbulence, several speckles could be seen, and  $N$  is the number of these speckles. We assume that these speckles fulfill two conditions [30]:

- (1) The speckles are independent of each other.
- (2) The phase distribution function is a Gaussian function related to  $\Delta_J$ .

Considering strong turbulence,  $N$  is larger  $1 \times 10^4$ . Thus, the integrals in Equation (12) are replaced by the summation in Equation (14).

$$\begin{cases} \chi_r \approx \frac{S}{N} \exp\left(-\frac{r_k^2}{\omega_a^2}\right) \sum_{k=1}^N \exp\left(-\frac{r_k^2}{\omega_a^2} + \frac{r_k^2}{\omega_a^2}\right) \cos \phi_k \\ \chi_i \approx \frac{S}{N} \exp\left(-\frac{r_k^2}{\omega_a^2}\right) \sum_{k=1}^N \exp\left(-\frac{r_k^2}{\omega_a^2} + \frac{r_k^2}{\omega_a^2}\right) \sin \phi_k \\ N = \left\{ 1.09 \left(\frac{r_0}{D}\right)^{\frac{1}{2}} \Gamma\left[\frac{6}{5}, 1.08 \left(\frac{D}{r_0}\right)^{\frac{5}{3}}\right] \right\}^{-1} \end{cases} \tag{14}$$

$N$  is large enough so that  $\chi_r$  and  $\chi_i$  are considered approaching jointly normal distribution. The PDF is shown in Equation (15).

$$p_{\chi_r, \chi_i}(\chi_r, \chi_i) = \frac{1}{2\pi\sigma_r\sigma_i} \exp\left[-\frac{(\chi_r - \bar{\chi}_r)^2}{2\sigma_r^2}\right] \exp\left[-\frac{(\chi_i - \bar{\chi}_i)^2}{2\sigma_i^2}\right] \tag{15}$$

$\bar{\chi}_r$  and  $\bar{\chi}_i$  are the mean value of  $\chi_r$  and  $\chi_i$ ,  $\sigma_r^2, \sigma_i^2$  represent the variance of  $\chi_r$  and  $\chi_i$ . Appendix A shows the calculation progress.

Substituting  $\chi_r = \sqrt{\chi^2} \cos\theta$  and  $\chi_i = \sqrt{\chi^2} \sin\theta$  into Equation (15) and integrating  $\theta$  from 0 to  $2\pi$ , the PDF of  $\chi^2$  is obtained shown by Equation (16).

$$p_{\chi^2} = \frac{1}{4\pi\sigma_r\sigma_i} \int_0^{2\pi} d\theta \exp\left[-\frac{(\chi\cos\theta - \bar{\chi}_r)^2}{2\sigma_r^2}\right] \exp\left[-\frac{(\chi\sin\theta)^2}{2\sigma_i^2}\right] \tag{16}$$

The modified Rician PDF [31] is a reasonable solution for Equation (16), shown in Equation (17), in which  $I_0(x)$  represents the first class modified Bessel functions.

$$\begin{cases} p_{\chi^2}(\chi^2) = \frac{1+c}{\chi^2} \exp(-c) \exp\left[-\frac{(1+c)\chi^2}{\chi^2}\right] I_0\left[2\chi\sqrt{\frac{(1+c)c}{\chi^2}}\right] \\ c = \left[\frac{\sigma_r^2 + \sigma_i^2 + \bar{\chi}^2}{\sqrt{\bar{\chi}_r^4 + 2\bar{\chi}_r^2(\sigma_i^2 - \sigma_r^2) - (\sigma_i^2 - \sigma_r^2)^2}} - 1\right]^{-1} \\ \chi^2 = \bar{\chi}_r^2 + \bar{\chi}_i^2 + \sigma_r^2 + \sigma_i^2 \end{cases} \tag{17}$$

After the Jacobian transformation, the PDF of CE is calculated, given by Equation (18). It has a simple analytic expression and is easily used for further application.

$$\begin{cases} p_H(\eta) = \frac{1+c}{\bar{\eta}} \exp(-c) \exp\left[-\frac{(1+c)\eta}{\bar{\eta}}\right] I_0\left[2\sqrt{\frac{(1+c)c\eta}{\bar{\eta}}}\right] \\ \bar{\eta} = \frac{2}{\pi^2 R^2 \omega_a^2} \chi^2 \end{cases} \tag{18}$$

All the algebraic operations above provide the statistical distribution of the CE under the condition of non-Kolmogorov turbulence. With rational assumptions, the PDF follows Rician distribution, which is beneficial to further study.

### 3. Simulation Analysis

In order to testify the PDF derived in Section 2, we simulated the model numerically by MATLAB.

Based on Equation (17), we notice that the PDF of the CE is related to its mean value and parameter  $c$ , both of which are the functions of  $\bar{\chi}_r$ ,  $\bar{\chi}_i$ ,  $\sigma_r^2$  and  $\sigma_i^2$ . It is necessary to calculate  $\bar{\chi}_r$ ,  $\bar{\chi}_i$ ,  $\sigma_r^2$  and  $\sigma_i^2$  before we simulate the PDF. According to Appendix A and ref. [32], the wavelength of the signal light ( $\lambda$ ), the pupil aperture of the receiving telescope ( $D$ ), the focal length of the coupling system ( $F$ ) and the model field diameter (MFD) of the SMF ( $d$ ) are the system parameters, while the atmospheric coherence length ( $r_0$ ) and  $\beta$  represent the turbulence conditions. All the parameters are necessary to simulate the statistical distribution of the CE.

The hierarchical map is shown in Figure 2. Firstly, one of the turbulence conditions should be decided as the variable, and the range should be chosen properly. With all the system parameters, the input of the simulation is prepared. Then, we calculate  $\bar{\chi}_r$ ,  $\bar{\chi}_i$ ,  $\sigma_r^2$  and  $\sigma_i^2$  for next processing. Based on the results,  $c$  and  $\bar{\eta}$  are calculated, and the PDF of the CE is derived. We can analyze the distribution of the CE within the range chosen before at last.

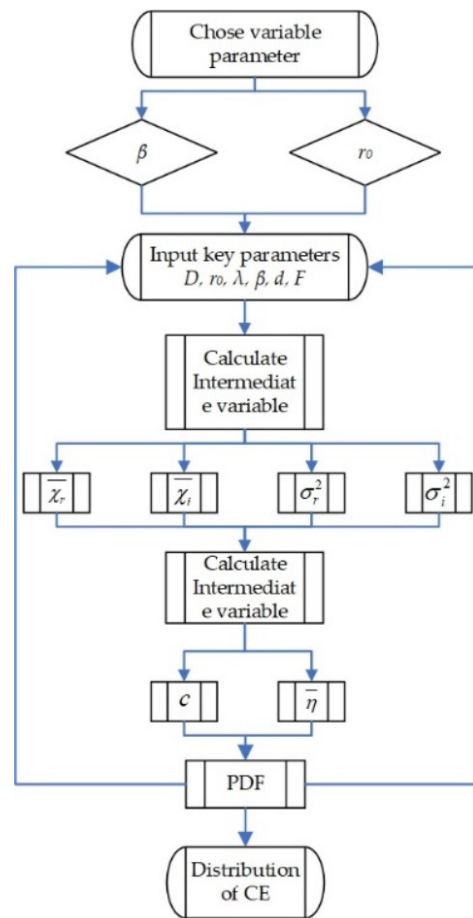


Figure 2. Hierarchical map of simulation progress.

The pseudo-code is listed in Algorithm 1.

**Algorithm 1:** The pseudo-code of the simulation progress

**Input:** System parameters and turbulence conditions ( $\lambda, D, F, d, r_0, \beta$ ).

**Output:** Distribution of CE

- 1: Choose variable parameter  $r_0$  (or  $\beta$ )
- 2: Initialize  $\lambda, D, F, d, \beta$  (or  $r_0$ ) with solid value.
- 3: Initialize  $r_0$  (or  $\beta$ ) with the range chosen properly
- 4:     **for** episode = 1, 2 . . . **do** as follows
- 5:         Calculate the intermediate variable  $\bar{\chi}_r, \bar{\chi}_i, \sigma_r^2$ , and  $\sigma_i^2$
- 6:         Calculate the intermediate variable  $c$  and  $\bar{\eta}$
- 7:         Analyze the PDF based the results of step 6
- 8:     **end for**
- 9:     Analyze the distribution of CE

The distribution of the CE was simulated in the conditions of the solid  $\beta$  with variable  $r_0$  and solid  $r_0$  with variable  $\beta$ . Here are the results.

3.1. Solid  $\beta$  with Variable  $r_0$

In this part, the PDF of the CE is discussed at the condition of variable  $r_0$  when  $D$  and  $\beta$  stay the same. The parameters are all listed in Table 3.

The atmospheric coherence length  $r_0$ , also known as Fried’s length, reflects the intensity of the atmospheric turbulence. With the growth of the turbulence,  $r_0$  gets smaller. Figure 3a–d show us the differences of the PDF of the CE when  $r_0$  varies from 0.1 m to 1 m. When the  $r_0$  equals to 0.1 m, shown by Figure 3a, the atmospheric turbulence is strong.

The PDF becomes nearly negatively exponentially distributed. This means that the mean value of the CE is quite small, so that the communication link is barely maintained. As the turbulence gets weaker,  $r_0$  becomes larger, from 0.2 m to 1 m. As presented in Figure 3b–d, a peak comes out at each curve of the PDF, and the distribution approximates the Rayleigh distribution. The average CE is larger, in which condition the communication is stabilized. Figure 4 gives a clear trend of the PDF of the CE.

**Table 3.** Analysis parameters at condition of solid  $\beta$  with variable  $r_0$ .

Items	Value
Wavelength ( $\lambda$ )	1550 nm
Pupil aperture ( $D$ )	1 m
Focal length of coupling system ( $F$ )	4.17 m
MFD of single-mode fiber ( $d$ )	5.5 $\mu$ m
Atmospheric coherence length ( $r_0$ )	0.1~1 m
$\beta$	11/3

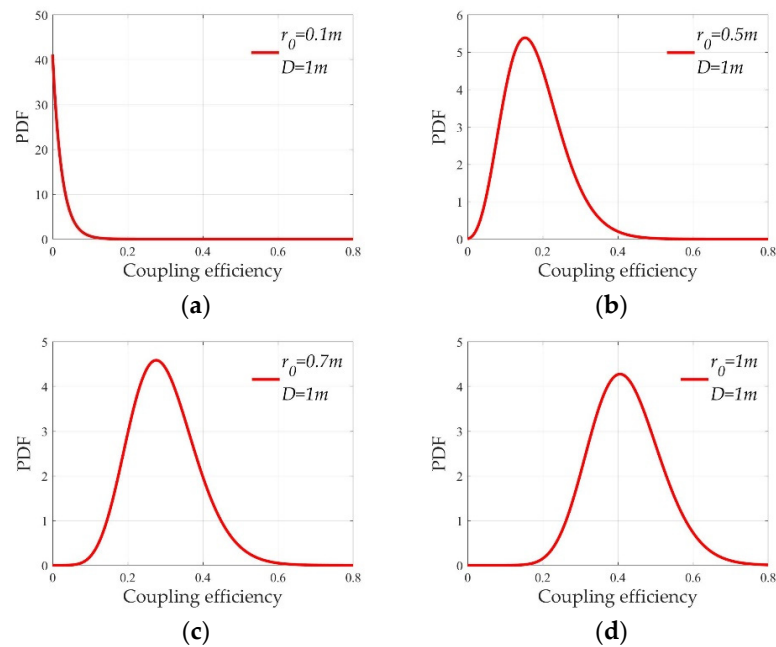


**Figure 3.** PDF of coupling efficiency with solid  $\beta$  and variable  $r_0$ . (a)  $r_0 = 0.1$  m; (b)  $r_0 = 0.5$  m; (c)  $r_0 = 0.7$  m; (d)  $r_0 = 1$  m.

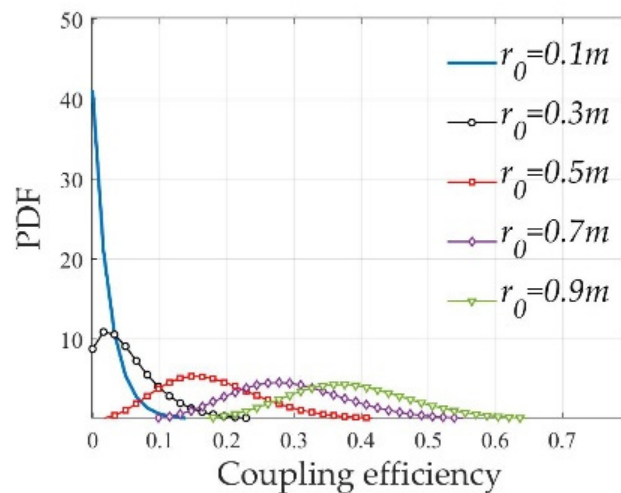


**Figure 4.** PDF of coupling efficiency as  $r_0$  varies from 0.1 m to 0.9 m.



The simulation shows that the modified Rician distribution describes the PDF of the CE well under the circumstance of both weak and strong turbulence, as shown by Figures 3 and 4. The model is extendable to the free-space optical communication system for further study.

### 3.2. Solid $r_0$ with Variable $\beta$

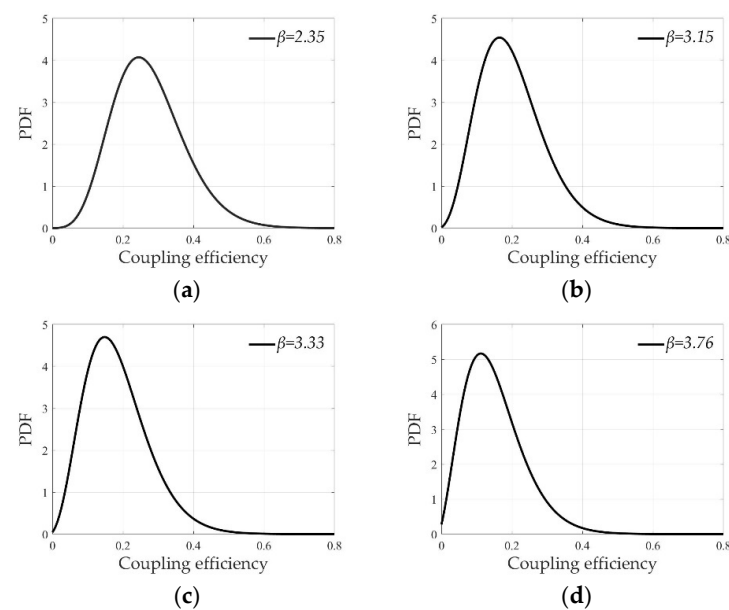
In this part, the PDF of the CE is discussed in the condition of variable  $\beta$  when  $D$  and  $r_0$  stay the same. The parameters are all listed in Table 4.

**Table 4.** Analysis parameters at condition of solid  $r_0$  with variable  $\beta$ .

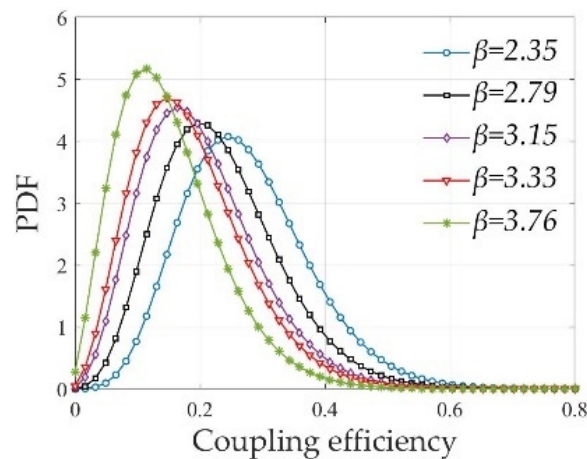
Items	Value
Wavelength ( $\lambda$ )	1550 nm
Pupil aperture ( $D$ )	1 m
Focal length of coupling system ( $F$ )	4.17 m
MFD of single-mode fiber ( $d$ )	5.5 $\mu\text{m}$
Atmospheric coherence length ( $r_0$ )	0.5 m
$\beta$	2.35~3.76

Figure 5a–d show the situation whereby the PDF of the CE changes with different  $\beta$  when  $r_0$  equals to 0.5 for the same receiving device. The result contains the case that  $\beta$  equals to 11/3, which means the Kolmogorov turbulence model is used. The curves in these pictures show that the distribution of the CE differs from each other. Figure 6 gives a clearer tendency of the changing PDF.

When the power law  $\beta$  has a slight change, the average value of the CE does not change much, but the distribution of the CE varies. This means that the variance of the wavefronts is different for each case, which will lead to different power fluctuations of communication terminals. In the free-space optical communication link though the atmosphere, non-Kolmogorov turbulence is improved by widely exiting, where  $\beta$  is not equal to 11/3 in all conditions. Kolmogorov theory could not describe turbulence at all conditions. It is not accurate to use one distribution to describe the fluctuation of the CE in different turbulence conditions. The statistical model of the coupling efficiency based on the non-Kolmogorov model is more accurate and necessary to evaluate the performance of the receiving device.



**Figure 5.** PDF of coupling efficiency with solid  $r_0$  and variable  $\beta$ . (a)  $\beta = 2.35$ ; (b)  $\beta = 3.15$ ; (c)  $\beta = 3.33$ ; (d)  $\beta = 3.76$ .



**Figure 6.** PDF of coupling efficiency as  $\beta$  varies from 2.7 to 3.76.

The simulation in this section indicates that the statistical model built for the CE has the robustness for both weak and strong turbulence. With the non-Kolmogorov turbulence applied, it allows the power law  $\beta$  to be alterable so that the theoretical distribution of the CE could change, which leads to an expendable application.

#### 4. Experimental Verification

##### 4.1. Experimental Instruments

We designed an experiment in the laboratory to verify the statistical model built in Section 2. Figure 7 shows the schematic diagram. An optical fiber collimator is linked to a fiber-output laser as the signal laser source. The divergence angle is not small enough so that telescope is applied as the beam expander. Transmitting through the turbulence generated by equipment 3, the laser beam is received by a telescope and then split into two beams by a BS. One is reflected into a wavefront sensor to calculate  $r_0$ , the other beam passes through the BS and incident into the coupling lens. An SMF is placed behind the lens on a six-axis stage to maximize the CE.

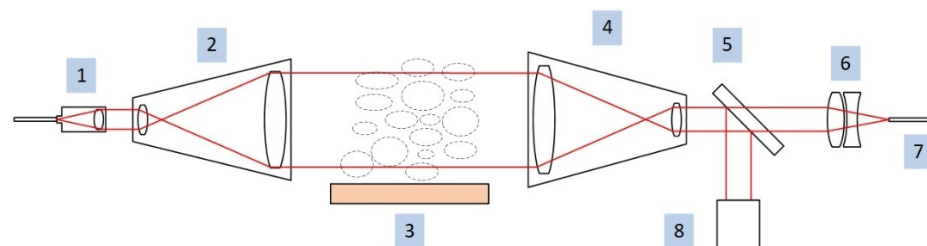


**Figure 7.** Schematic diagram of the experiment. 1—optical fiber collimator, 2—beam expander, 3—turbulence generator, 4—receiving telescope, 5—beam splitter, 6—coupling lens, 7—SMF, 8—wavefront sensor.

The layout of the experiment is shown in Figure 8a. A fiber collimator linked to a fiber-output laser with the wavelength of 1550 nm is put at position 1, while the light source and its divergence angle is 1.2 mrad. Expanded by a beam expander consisting of a set of lenses placed in position 2 and 4, the emergent beam transmits through the turbulence. A heat gun with a designed air outlet is set at position 5 as the turbulence generator. The wind speed and temperature are adjustable to control the intensity of the turbulence. The lenses placed at positions 10 and 15 form the receiving telescope. A BS is laid at position 13 to split the incident beam. One of the split beams is received by a Hartmann–Shack wavefront sensor placed behind the BS at position 14 to measure  $r_0$ , and the other is reflected by some mirrors and transmitted into a set of lenses used as the coupling lens at position 19. An SMF is set at a six-axis stage behind the coupling lenses and linked to an optical power meter.

The data are essential to calculate the CE and analyze its statistical distribution. Figure 8b shows the details of the coupling parts, marked with a green dashed line in Figure 8a. All the mirrors shown in Figure 8a are used for bending the optical path. Moreover, the experiment is also set to verify the tracking algorithm designed for an FSO system, so some FMSs are laid in the optical path. During the experiment for this paper, all the FMSs were frozen at a certain position and will not introduce extra errors.

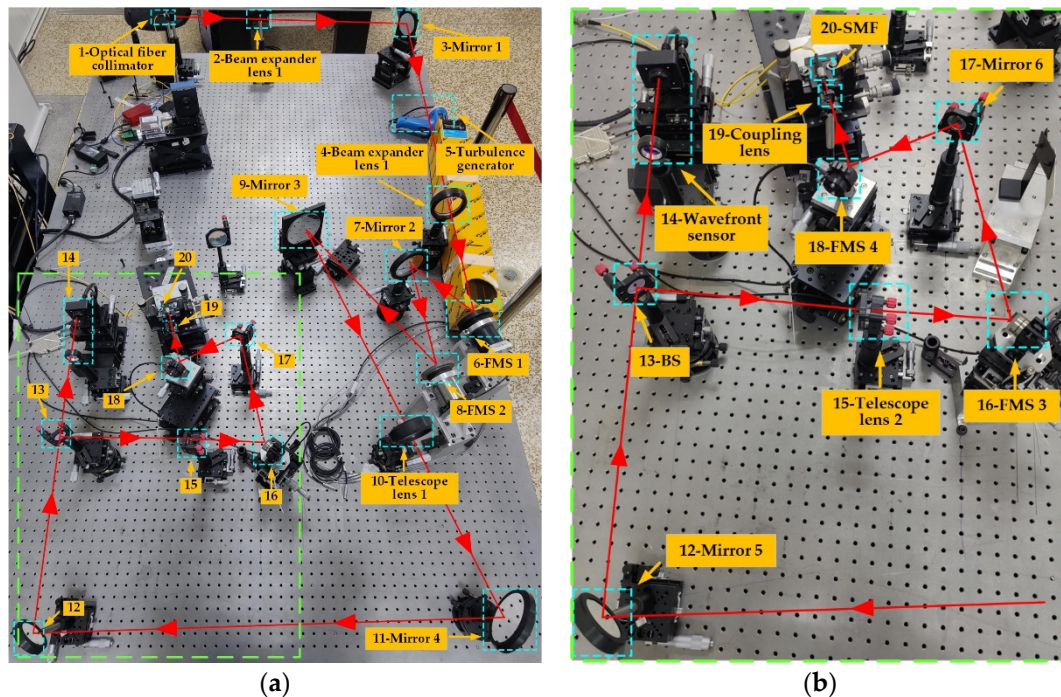


**Figure 8.** Experimental layout. (a) overall layout, (b) SMF coupling system.

Table 5 shows the key parameters of the equipment related to the experiment.

**Table 5.** Key parameters of the experimental system.

Items	Value
Wavelength	$1550 \pm 0.5$ nm
Divergence angle of the fiber collimator	1.2 mrad
Magnification of beam expander system (2 and 4)	10 $\times$
Diameter of coupling lens	12.7 mm
Focal length of coupling lens	53 mm
Magnification of the receiving telescope (10 and 15)	1/3 $\times$
Single-mode fiber	Corning SMF-28e

#### 4.2. Results and Discussion

We measured the optical power of the incident beam before the coupling lens and an optical power meter was connected with the SMF so that the CE affected by turbulence could be calculated. The  $r_0$  was analyzed using a wavefront reconstruction algorithm based on the data from the wavefront sensor. We counted the CE and normalized it with theoretical PDF, as shown in Figure 9a–e. The green dotted line represented the experimental CE, the blue line was for the theoretical PDF built with the Kolmogorov model and the red line was for the PDF using the non-Kolmogorov model. In order to evaluate the accuracy of the PDF, we calculated the correlation coefficient with the experimental distribution. The results are shown in Table 6.

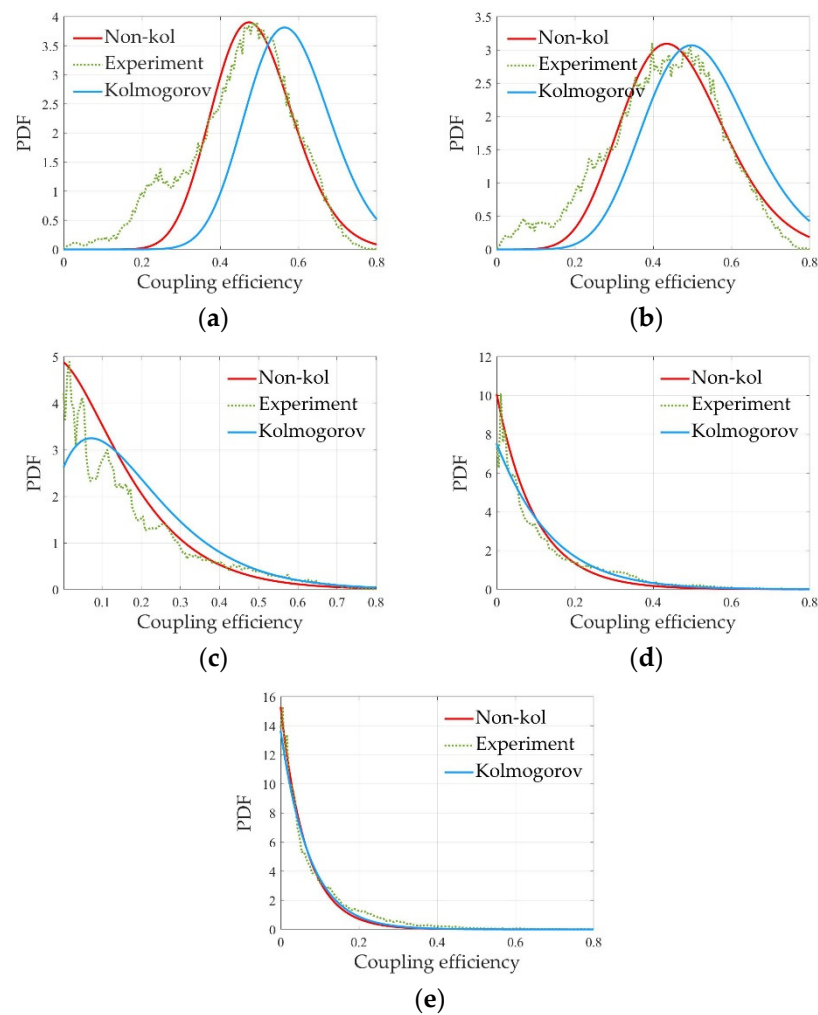


**Figure 9.** Experimental distribution fits theoretical distribution based on non-Kolmogorov model and Kolmogorov model. (a)  $r_0 = 0.136$  m; (b)  $r_0 = 0.104$  m; (c)  $r_0 = 0.034$  m; (d)  $r_0 = 0.023$  m; (e)  $r_0 = 0.017$  m.

**Table 6.** Correlation coefficients of experimental distribution and theoretical PDFs.

$r_0$ (m)	Non-Kolmogorov Model		Kolmogorov Model
	$\beta$	Correlation Coefficients	Correlation Coefficients
0.134	2.79	0.9765	0.6546
0.105	2.89	0.9537	0.8378
0.035	3.78	0.9783	0.9213
0.023	3.95	0.9898	0.9762
0.016	3.61	0.9945	0.9908

As observed in Table 6,  $r_0$  ranges from 0.134 m down to 0.016 m, which means that the atmospheric turbulence gets stronger. In Figure 9a, the  $r_0$  equals to 0.134 m, whereby the turbulence was weak compared with the diameter of receiving aperture, so that the CE distributed mainly between 0.2 and 0.6. When the  $r_0$  came to 0.016, as shown in Figure 9e, the CE distributed only between 0 and 0.2, in which case the intensity of the turbulence was strong. The PDF of the CE based on the Kolmogorov model and the non-Kolmogorov model was calculated. As shown in Figure 9a–c, the correlation coefficients using the non-Kolmogorov model were all greater than 0.95, which comes to 0.9898 in Figure 9d. On the contrary, the correlation coefficients using the Kolmogorov model were less than 0.9 and only equaled to 0.6546 in Figure 9a. As to Figure 9d,e, the correlation coefficients were all greater than 0.9, no matter whether the PDFs were built on the non-Kolmogorov

model or the Kolmogorov model. This means that the PDFs built on the non-Kolmogorov model fit the experimental distribution better than those built on the Kolmogorov models, whether the turbulence was strong or weak.

The results listed in Table 6 and shown in Figure 9a–e indicate that the Kolmogorov model is not suitable for all cases, for it has strong boundary conditions. When the Kolmogorov model is used, it is assumed that the eddies of the turbulence are much smaller than its outer scale and much bigger than its inner scale. What is more, the eddies that belong to the turbulence should be statistically homogeneous and isotropic. It is difficult to find such conditions in actual communication links, especially in cities where human activities are complex and massive. Taking this experiment for example, we used a heat gun to generate turbulence in a small region, and the energy injected did not spread equally during the short time, especially when the wind speed and temperature were both high. The boundary condition of the Kolmogorov model was not suitable in this case, so the PDF built on the Kolmogorov model did not fit the experimental distribution. However, when the power law  $\beta$  was introduced in the turbulence model, as non-Kolmogorov turbulence emerged, the variance of the wavefront was properly corrected, and the PDF fit the experimental distribution. In the condition of strong turbulence, the variances of the wavefront for the different  $\beta$  were approximately equal, so the PDF built on the Kolmogorov model and the non-Kolmogorov model were both applicable. The results showed the robustness of the statistical model of the CE. Therefore, the PDF based on the non-Kolmogorov turbulence model was more accurate to describe the statistical properties of the random CE introduced by atmospheric turbulence.

## 5. Conclusions

In this paper, we created a new statistical model of the CE based on the non-Kolmogorov turbulence theory. The power law  $\beta$  was introduced as a correction factor so that the variance of the wavefront residual variance could fit the actual distribution. A numerical simulation was done to test its robustness and rationality. The results showed that the statistical model was suitable for both weak and strong turbulence because the  $\beta$  was not constant. Finally, we set up an experiment to verify the statistical model. After counting the CE data, we found that the PDF built on the non-Kolmogorov turbulence model suited the experimental distribution well, because  $\beta$  was variable, and so we could choose a proper value so that variance of the wavefront was corrected. In conclusion, the statistical model of the CE based on non-Kolmogorov turbulence could describe the distribution of the CE well in the presence of atmospheric turbulence. With the application of this model, it is beneficial to evaluate the properties of the FSO terminals so to reduce the design costs at the beginning. Further study should focus on choosing a proper  $\beta$  in different conditions.

**Author Contributions:** Conceptualization, L.M.; methodology, S.G.; software, L.M.; validation, S.G. and Y.L.; formal analysis, L.M.; investigation, L.M.; resources, S.G.; data curation, L.M. and Y.L.; writing—original draft preparation, L.M.; writing—review and editing, L.M. and B.C.; visualization, L.M. and B.C.; supervision, S.G.; project administration, S.G.; funding acquisition, S.G. All authors have read and agreed to the published version of the manuscript.

**Funding:** This research received no external funding.

**Institutional Review Board Statement:** Not applicable.

**Informed Consent Statement:** Not applicable.

**Conflicts of Interest:** The authors declare no conflict of interest.

**Appendix A. Calculation of  $\overline{\chi_r}$ ,  $\overline{\chi_i}$ ,  $\sigma_r^2$  and  $\sigma_i^2$**

According to the definition of  $\chi_r$  and  $\chi_i$ , and replacing  $-\frac{r_k^2}{\omega_0^2}$  with  $\Lambda_k$  for convenience, Equation (9) could be written as Equation (A1)

$$\begin{cases} \chi_r \approx \frac{S}{N} \exp(\overline{\Lambda_k}) \sum_{k=1}^N \exp(\Lambda - \overline{\Lambda_k}) \cos \phi_k \\ \chi_i \approx \frac{S}{N} \exp(\overline{\Lambda_k}) \sum_{k=1}^N \exp(\Lambda - \overline{\Lambda_k}) \sin \phi_k \\ N = \left\{ 1.09 \left(\frac{r_0}{D}\right)^{\frac{1}{2}} \Gamma \left[ \frac{6}{5}, 1.08 \left(\frac{D}{r_0}\right)^{\frac{5}{3}} \right] \right\}^{-1} \end{cases} \quad (A1)$$

After some algebraic calculus, the mean value of  $\chi_r$  and  $\chi_i$ , which are  $\overline{\chi_r}$  and  $\overline{\chi_i}$ , is given by Equation (A2), and the variance, which are  $\sigma_r^2$  and  $\sigma_i^2$ , is shown in Equation (A3).

$$\begin{cases} \overline{\chi_r} = \frac{S}{2} \exp(\overline{\Lambda_k}) \overline{\exp(\Lambda_k - \overline{\Lambda_k})} [M_\phi(1) + M_\phi(-1)] \\ \overline{\chi_i} = -\frac{iS}{2} \exp(\overline{\Lambda_k}) \overline{\exp(\Lambda_k - \overline{\Lambda_k})} [M_\phi(1) - M_\phi(-1)] \end{cases} \quad (A2)$$

$$\begin{cases} \frac{\sigma_r^2}{S} = \frac{\exp(2\overline{\Lambda_k}) \overline{\exp 2(\Lambda_k - \overline{\Lambda_k})}}{4N} [2 + M_\phi(2) + M_\phi(-2)] \\ - \frac{\exp(2\overline{\Lambda_k}) [\overline{\exp(\Lambda_k - \overline{\Lambda_k})}]^2}{4N} [2M_\phi(1)M_\phi(-1) + M_\phi^2(1) + M_\phi^2(-1)] \\ \frac{\sigma_i^2}{S} = \frac{\exp(2\overline{\Lambda_k}) \overline{\exp 2(\Lambda_k - \overline{\Lambda_k})}}{4N} [2 - M_\phi(2) - M_\phi(-2)] \\ - \frac{\exp(2\overline{\Lambda_k}) [\overline{\exp(\Lambda_k - \overline{\Lambda_k})}]^2}{4N} [2M_\phi(1)M_\phi(-1) - M_\phi^2(1) - M_\phi^2(-1)] \end{cases} \quad (A3)$$

$M_\phi(\omega)$  is the Fourier transformation of the PDF of the random phase  $\phi$ . Based on central-limit theorem, the random phase  $\phi$  follows the standard normal distribution, so  $M_\phi(\omega)$  is given by Equation (A4).

$$M_\phi(\omega) = \exp\left(-\frac{\sigma_\phi^2 \omega^2}{2}\right) \quad (A4)$$

$\sigma_\phi^2$  is the variance of phase  $\phi$ . When the wavefront is expanded by the infinite Zernike terms, and the first  $J$  terms are corrected,  $\sigma_\phi^2$  is equal to  $\Delta_J$ , shown as Equation (6)

After massive algebraic calculus, Equations (A2) and (A3) is expressed as Equations (A5) and (A6).

$$\begin{cases} \overline{\chi_r} = S \exp(\overline{\Lambda_k}) \overline{\exp(\Lambda_k - \overline{\Lambda_k})} \exp\left(-\frac{\sigma_\phi^2}{2}\right) \\ \overline{\chi_i} = 0 \end{cases} \quad (A5)$$

$$\begin{cases} \frac{\sigma_r^2}{S} = \frac{\exp(2\overline{\Lambda_k}) \overline{\exp 2(\Lambda_k - \overline{\Lambda_k})}}{2N} [1 + \exp(-2\sigma_\phi^2)] - \frac{\exp(2\overline{\Lambda_k}) [\overline{\exp(\Lambda_k - \overline{\Lambda_k})}]^2}{N} \exp(-\sigma_\phi^2) \\ \frac{\sigma_i^2}{S} = \frac{\exp(2\overline{\Lambda_k}) \overline{\exp 2(\Lambda_k - \overline{\Lambda_k})}}{2N} [1 - \exp(-2\sigma_\phi^2)] \end{cases} \quad (A6)$$

Considering the atmospheric channel, the area that the signal light covers at the optical pupil of the receiving telescope is much larger than the aperture, so we assume that the speckles spread equally at this small area and follow a uniform distribution. Thus,  $r_k$  follows a 2-dimensional uniform distribution, as shown in Equation (A7).

$$p_{R_k}(r_k) = \begin{cases} \frac{1}{\pi R^2}, & |r_k| \leq R \\ 0, & |r_k| \geq R \end{cases} \quad (A7)$$

As a result, the expressions of  $\overline{\Lambda_k}$ ,  $\overline{\exp(\Lambda_k - \overline{\Lambda_k})}$  and  $\overline{\exp 2(\Lambda_k - \overline{\Lambda_k})}$  are given by Equations (A8)–(A10), respectively.

$$\overline{\Lambda_k} = 2\pi \int_0^R \left( -\frac{r_k^2}{\omega_a^2} \right) \cdot \frac{1}{\pi R^2} \cdot r_k dr_k = -\frac{R^2}{2\omega_a^2} \quad (\text{A8})$$

$$\begin{aligned} \overline{\exp(\Lambda_k - \overline{\Lambda_k})} &= \frac{\exp(\Lambda_k)}{\exp(\overline{\Lambda_k})} = \frac{2\pi}{\exp(\overline{\Lambda_k})} \int_0^R \exp\left(-\frac{r_k^2}{\omega_a^2}\right) \cdot \frac{1}{\pi R^2} \cdot r_k dr_k \\ &= \frac{\omega_a^2}{R^2} \left[ 1 - \exp\left(-\frac{R^2}{\omega_a^2}\right) \right] / \exp\left(-\frac{R^2}{2\omega_a^2}\right) \end{aligned} \quad (\text{A9})$$

$$\begin{aligned} \overline{\exp 2(\Lambda_k - \overline{\Lambda_k})} &= \frac{\exp(2\Lambda_k)}{\exp(2\overline{\Lambda_k})} = \frac{2\pi}{\exp(2\overline{\Lambda_k})} \int_0^R \exp\left(-\frac{2r_k^2}{\omega_a^2}\right) \cdot \frac{1}{\pi R^2} \cdot r_k dr_k \\ &= \frac{\omega_a^2}{2R^2} \left[ 1 - \exp\left(-\frac{2R^2}{\omega_a^2}\right) \right] / \exp\left(-\frac{R^2}{\omega_a^2}\right) \end{aligned} \quad (\text{A10})$$

Thus, the value of  $\overline{\chi_r}$ ,  $\overline{\chi_i}$ ,  $\sigma_r^2$  and  $\sigma_i^2$  are shown by Equations (A11) and (A12).

$$\begin{cases} \overline{\chi_r} = \pi\omega_a^2 \left[ 1 - \exp\left(-\frac{R^2}{\omega_a^2}\right) \right] \exp\left(-\frac{\sigma_\phi^2}{2}\right) \\ \overline{\chi_i} = 0 \end{cases} \quad (\text{A11})$$

$$\begin{cases} \sigma_r^2 = \frac{\pi\omega_a^2}{4N} \left[ 1 - \exp\left(-\frac{2R^2}{\omega_a^2}\right) \right] \left[ 1 + \exp\left(-2\sigma_\phi^2\right) \right] - \frac{\pi\omega_a^4}{NR^2} \left[ 1 - \exp\left(-\frac{R^2}{\omega_a^2}\right) \right]^2 \exp\left(-\sigma_\phi^2\right) \\ \sigma_i^2 = \frac{\pi\omega_a^2}{4N} \left[ 1 - \exp\left(-\frac{2R^2}{\omega_a^2}\right) \right] \left[ 1 - \exp\left(-2\sigma_\phi^2\right) \right] \end{cases} \quad (\text{A12})$$

## References

- Hauschildt, H.; Elia, C. Esas scylight programme: Activities and status of the high throughput optical network “hydron”. *Proc. SPIE* **2018**, *11180*, 111800G-1–111800G-8.
- Toyoshima, M. Recent trends in space laser communications for small satellites and constellations. *J. Lightwave Technol.* **2021**, *39*, 693–699. [[CrossRef](#)]
- Saathof, R. Optical satellite communication space terminal technology at tno. *Proc. SPIE* **2018**, *11180*, 111800K-1–111800K-10.
- Andrews, L.C.; Phillips, R.L. *Laser Beam Propagation through Random Media*, 2nd ed.; SPIE: Bellingham, WA, USA, 2005; pp. 57–60.
- Dikmelik, Y.; Davidson, F.M. Fiber-coupling efficiency for free-space optical communication through atmospheric turbulence. *Appl. Opt.* **2005**, *44*, 4946–4952. [[CrossRef](#)]
- Du, W.; Yuan, Q. Scintillation index of a spherical wave propagating through Kolmogorov and non-Kolmogorov turbulence along laser-satellite communication uplink at large zenith angles. *J. Russ. Laser Res.* **2021**, *42*, 198–209. [[CrossRef](#)]
- Be1en’kii, M.S.; Karis, S.J.; Brown, J.M.; Fugate, R.Q. Experimental evidence of the effects of non-Kolmogorov turbulence and anisotropy of turbulence. *Proc. SPIE* **1999**, *3749*, 50–51.
- Wang, G. A new random-phase-screen time series simulation algorithm for dynamically atmospheric turbulence wave-front generator. *Proc. SPIE* **2006**, *6027*, 602716.
- Wu, X.; Huang, Y.; Mei, H.; Shao, S.; Huang, H.; Qian, X.; Cui, C. Measurement of non-Kolmogorov turbulence characteristic parameter in atmospheric surface layer. *Acta Opt. Sin.* **2014**, *34*, 0601001.
- Cui, L.Y.; Xue, B.D. Influence of moderate-to-strong non-Kolmogorov turbulence on the imaging system by atmospheric turbulence MTF. *Optik* **2015**, *126*, 191–198. [[CrossRef](#)]
- Baykal, Y. Coherence length in non-Kolmogorov satellite links. *Opt. Commun.* **2013**, *308*, 105–108. [[CrossRef](#)]
- Yao, J.R. Oceanic non-Kolmogorov optical turbulence and spherical wave propagation. *Opt. Express* **2021**, *29*, 1340–1359. [[CrossRef](#)] [[PubMed](#)]
- El-Nahal, F.I. Coherent quadrature phase shift keying optical communication systems. *Optoelectron. Lett.* **2018**, *14*, 0372–0375. [[CrossRef](#)]
- Hu, B.; Zhang, Y. New model of the fiber coupling efficiency of a partially coherent Gaussian beam in an ocean to fiber link. *Opt. Express* **2018**, *26*, 25111–25119. [[CrossRef](#)]
- Chen, X.; Hu, X. High coupling efficiency technology of large core hollow-core fiber with single mode fiber. *Opt. Express* **2019**, *27*, 33135–33142. [[CrossRef](#)] [[PubMed](#)]
- Liu, N.; Zhang, J.; Zhu, Z. Efficient coupling between an integrated photonic waveguide and an optical fiber. *Opt. Express* **2021**, *29*, 27396–27403. [[CrossRef](#)] [[PubMed](#)]
- Chahine, Y.K.; Wroblewski, A.C. Laser beam propagation simulations of long-path scintillation and fade with comparison to ground-to-aircraft optical link measurements. *Opt. Eng.* **2021**, *60*, 036112-1–036112-15. [[CrossRef](#)]

18. Farid, A.A. Outage capacity optimization for free-space optical links with pointing errors. *J. Lightwave Technol.* **2007**, *25*, 1702–1710. [[CrossRef](#)]
19. Zhai, C.; Tan, L. Fiber coupling efficiency for a Gaussian-beam wave propagating through non-Kolmogorov turbulence. *Opt. Express* **2015**, *23*, 15242–15255. [[CrossRef](#)]
20. Zhai, C.; Tan, L. Fiber coupling efficiency in non-Kolmogorov satellite links. *Opt. Commun.* **2015**, *336*, 93–97. [[CrossRef](#)]
21. Hua, B.; Xu, Y. Coupling efficiency of a partially coherent laser beam from the anisotropy and non-Kolmogorov marine-atmosphere turbulence to fiber. *Optik* **2019**, *183*, 1–6. [[CrossRef](#)]
22. Zhao, X.; Jiang, H.; Han, C. Fiber coupling efficiency on focal plane spot extension caused by turbulence. *Optik* **2013**, *124*, 1113–1115. [[CrossRef](#)]
23. Wang, C.; Jiang, L. Fiber-coupling efficiency for a Gaussian-beam wave passing through weak fluctuation regimes. *J. Laser Appl.* **2017**, *29*, 032001-1–032001-7. [[CrossRef](#)]
24. Chen, M.; Liu, C. Experimental demonstration of single-mode fiber coupling over relatively strong turbulence with adaptive optics. *Appl. Opt.* **2015**, *54*, 8722–8726. [[CrossRef](#)] [[PubMed](#)]
25. Bian, Y.; Li, Y. Free-space to single-mode fiber coupling efficiency with optical system aberration and fiber positioning error under atmospheric turbulence. *J. Opt.* **2022**, *24*, 025703. [[CrossRef](#)]
26. Li, Y.; Zhu, W. Equivalent refractive-index structure constant of non-Kolmogorov turbulence. *Opt. Express* **2015**, *23*, 23004–23012. [[CrossRef](#)]
27. Zeng, A.P.; Huang, Y.P. Spreading of partially coherent polychromatic Hermite-Gaussian beams propagating through non-Kolmogorov turbulence. *Opt. Commun.* **2012**, *285*, 4825–4830. [[CrossRef](#)]
28. Robert, J. Noll Zernike polynomials and atmospheric turbulence. *J. Opt. Soc. Am.* **1976**, *66*, 207–211.
29. Boreman, G.D.; Dainty, C. Zernike expansions for non-Kolmogorov turbulence. *J. Opt. Soc. Am. A* **1996**, *13*, 517–522. [[CrossRef](#)]
30. Cagigal, M.P.; Canales, V.F. Speckle statistics in partially corrected wave fronts. *Opt. Lett.* **1998**, *23*, 1072–1074. [[CrossRef](#)]
31. Jing, M.; Lie, M. Statistical model of the efficiency for spatial light coupling into a single-mode fiber in the presence of atmospheric turbulence. *Appl. Opt.* **2015**, *54*, 9287–9293.
32. Jing, M.; Fang, Z. Plane wave coupling into single-mode fiber in the presence of random angular jitter. *Appl. Opt.* **2009**, *48*, 5184–5189.